LAWRENCE
LIVERMORE
NATIONAL
LABORATORY

UCRL-TR-234617

Implementation of Energy-Dependent Q Values for Fission

B. Beck, D. A. Brown, F. Daffin, J. Hedstrom, R. Vogt

September 14, 2007

This work was performed under the auspices of the U.S. Department of Energy by University of California, Lawrence Livermore National Laboratory under Contract W-7405-Eng-48.

Implementation of Energy-Dependent Q Values for Fission*

B. Beck, D. A. Brown, F. Daffin, J. Hedstrom and R. Vogt

Lawrence Livermore National Laboratory
P. O. Box 808
Livermore, California 94551

We discuss how the fission Q values for ^{235}U, ^{238}U and ^{239}Pu depend on the energy of the incident neutron. We then describe how these values have been implemented in `mcfgen` etc.

^{0*}This work was performed under the auspices of the U.S. Department of Energy by University of California, Lawrence Livermore National Laboratory under Contract W-7405-Eng-48. R.V. was supported in part by the National Science Foundation Grand NSF PHY-0555660.

1 Introduction

This paper describes the calculation of energy-dependent fission Q values by Madland [1] and explains how it has been implemented in the ENDL database for use in the LLNL codes.

Until now the fission Q value in the ENDL database has been assumed to be a constant 180 MeV. However, it is reasonable to expect that the Q value changes as a function of incident energy. While binary fission is most probable for all energies, symmetric binary fission becomes more probable with increasing incident energy. Higher incident energy can lead to more highly excited fission fragments, leading in turn to larger prompt neutron and gamma emission from the excited fragments. These effects all suggest that the fission Q value is energy dependent. Madland's paper attempts to quantify this energy dependence using parameterizations based on fits to data and the Los Alamos (Madland-Nix) model [2].

The parameterizations by Madland are for three isotopes only: two of uranium, ^{235}U and ^{238}U, and one of plutonium, ^{239}Pu. While these three are of major importance for applications, other fissionable isotopes may be of interest in the future. For these, an alternative solution needs to be found. In addition, since the parameterizations here are based on averages only, they cannot be applied on an event-by-event basis since the Q depends not only on the incident energy of the neutron inducing the fission but also on the identity of the nuclear fragments. These correlations are beyond the scope of this work.

There are several stages in a fission event, depending on the time scale. Neutrons and gammas may be emitted at any time during the fission event. While our discussion here is focussed on compound nucleus creation by an incident neutron, similar parameterizations could be obtained for incident gammas or spontaneous fission.

Before the fission occurs, the excited compound nucleus of mass A and charge Z created by the interaction of an incident neutron, n, of mass m_n and carrying energy E_n, with a target of mass $A-1$ and charge Z, can emit one or more neutrons. These neutrons are referred to as 'pre-scission' neutrons. If one pre-scission neutron is emitted, the subsequent fission is referred to as 'second chance' fission since fission without any pre-scission neutron emission is 'first-chance' fission. Likewise, if two pre-scission neutrons are emitted, the fission event is 'third-chance' fission. Pre-scission emission reduces the energy available to the system after fission occurs. The incident energy needs to be rather high for second and third-chance fission to be significant.

After the compound nucleus has been formed, it has kinetic energy T and excited mass $M^*(Z,A)$. We neglect pre-scission neutron emission and assume binary fission of the compound nucleus into a light, L, and a heavy, H, fragment, both having kinetic energy T_i and excited mass M_i^*. After the fission, when the identity of the light and heavy fragments has been fixed, the excited fragments will decay to the ground state by neutron and gamma

emission. The fragment decay time is relatively short. Thus the neutrons and gammas emitted during the decay process are referred to 'prompt' neutrons and gammas.

Neutron emission typically occurs first, on a shorter time scale, $10^{-18} - 10^{-13}$ s, while the fragment excitation energy is above the neutron separation energy, S_n. Neutron emission will change the mass number of the initial fragment from A_i to $\tilde{A}_i$. Thus if the number of neutrons emitted by the decay of fragment i is denoted as ν_i, the baryon number of product i is

$$\tilde{A}_i = A_i - \nu_i \ . \tag{1}$$

We note that as the fragment A changes, the neutron separation energy may differ between *e.g.* A_i and $A_i - 1$ so that the number of emitted neutrons is very sensitive to the initial fragment identity. Gamma emission is responsible for the de-excitation of $\tilde{A}_i$ to its ground state for excitation energies less than the neutron separation energy over a time scale of $10^{-14} - 10^{-7}$ s. This is the end of the prompt fission energy release. Note that while the A of the fragment has changed, Z_i remains the same throughout the prompt stage. After prompt neutron and gamma emission is finished, the residual nuclei are referred to as fission 'products' rather than fragments, a term reserved for the nuclei produced in the binary fission process in Madland's presentation. The prompt neutron multiplicity that can be obtained from Madland's parameterizations includes the emission from both fission fragments. In addition, Madland's gamma energy includes all gamma emission during the time scale of the measurement (including any emitted pre-scission).

On a longer time scale, from a few milliseconds to minutes (or years, depending on when the observation is made), the fission products can emit further, 'delayed' neutrons and gammas, changing $\tilde{A}_i$ further. In addition, the product nuclei can beta decay, changing Z_i. Since delayed emission accounts for only a very small fraction of both the neutron multiplicity and the fission energy release, it is not considered in Madland's parameterization.

The prompt fission energy release is obtained by conservation of energy,

$$\begin{aligned} T + M^*(Z,A) &= E_n + m_n + M(Z, A-1) && (2) \\ &= T_L(Z_L, A_L) + M^*_L(Z_L, A_L) \\ &\quad + T_H(Z_H, A_H) + M^*_H(Z_H, A_H) \ . && (3) \end{aligned}$$

The excited mass of the compound nucleus and the fragments includes the ground state masses M and the excitation energy E^*,

$$M^* = M + E^* \ . \tag{4}$$

The initial fragments conserve baryon number and charge,

$$\begin{aligned} A &= A_L + A_H \ , && (5) \\ Z &= Z_L + Z_H \ . && (6) \end{aligned}$$

After the fission, when the identity of the light and heavy fragments has been fixed, the excited fragments will decay to the ground state by neutron and gamma emission.

The Q value of neutron capture for the compound nucleus formation,

$$m_n + M(Z, A-1) = M(Z, A) + B_n \ , \tag{7}$$

can be used to determine the binding energy of the neutron in the compound nucleus. Inserting Eq. (7) into Eq. (3) gives

$$\begin{aligned} E_n + B_n + M(Z,A) &= T_L(Z_L, A_L) + M_L(Z_L, A_L) + E^*_L(Z_L, A_L) \\ &\quad + T_H(Z_H, A_H) + M_H(Z_H, A_H) + E^*_H(Z_H, A_H) \ . \end{aligned} \tag{8}$$

Ideally, the total fission energy release is simply the difference in ground state masses of the compound nucleus and the fission fragments,

$$E_r = M(Z,A) - M_L(Z_L, A_L) - M_H(Z_H, A_H) \ . \tag{9}$$

Rearranging Eq. (8), the energy release can be written in terms of the light and heavy fragment kinetic and excitation energies,

$$\begin{aligned} E_r &= T_L(Z_L, A_L) + T_H(Z_H, A_H) \\ &\quad + E^*_L(Z_L, A_L) + E^*_H(Z_H, A_H) - E_n - B_n \ . \end{aligned} \tag{10}$$

By combining the fragment kinetic energies into a single value, $T_f^{\rm tot}$, and the excitation energies into the value $E^*_{\rm tot}$, Eq. (10) can be written more compactly as

$$E_r = T_f^{\rm tot} + E^*_{\rm tot} - E_n - B_n \tag{11}$$

where

$$T_f^{\rm tot} = T_L(Z_L, A_L) + T_H(Z_H, A_H) \ , \tag{12}$$

$$E^*_{\rm tot} = E^*_L(Z_L, A_L) + E^*_H(Z_H, A_H) \ . \tag{13}$$

We note that all quantities in Eqs. (11)-(13) depend on the incident neutron energy E_n. However, to keep the notation less cumbersome, we do not include this dependence explicitly in the text.

In reality, the situation is more complicated since binary fission occurs through a wide range of final states so that the identities of the light and heavy fragments are unknown. Indeed, a compound nucleus fissions into an array of possible fragments with the baryon of one fragment in the range $70 < A_f < 170$. In addition, 4-5 nuclei of different Z can have the same A_f. Furthermore, it is not possible to identify the fission fragments, only the fission products later in time. Parameterizations based on data are only knowable on average. Thus the energy release, the fission product kinetic energy and the excitation energy in Eq. (11) are replaced with their average

values. The average is found by weighting with the fragment yield, Y_f, where $Y_L = Y_H$ can be factored out so that

$$\begin{aligned}
\langle E_r \rangle &= \langle T_f^{\rm tot} \rangle + \langle E_{\rm tot}^* \rangle - E_n - B_n \ , & (14)\\
&= M(Z,A) - \frac{\sum [Y_f][M_L(Z_L,A_L) + M_H(Z_H,A_H)]}{\sum Y_f} & (15)\\
\langle T_f^{\rm tot} \rangle &= \frac{\sum [Y_f][T_L(Z_L,A_L) + T_H(Z_H,A_H)]}{\sum Y_f} \ , & (16)\\
\langle E_{\rm tot}^* \rangle &= \frac{\sum [Y_f][E_L^*(Z_L,A_L) + E_H^*(Z_H,A_H)]}{\sum Y_f} \ . & (17)
\end{aligned}$$

While the fission fragment kinetic energy enters Eq. (14), the fission product kinetic energy is measured. The two differ by the kinetic energies of the emitted neutrons. Thus if *e.g.* the light fragment emits $\overline{\nu}_L$ prompt neutrons, the kinetic energy of the light fragment becomes

$$T_L' = T_L \frac{\tilde{A}_L}{A_L} = T_L \frac{A_L - \overline{\nu}_L}{A_L} = T_L \Big(1 - \frac{\overline{\nu}_L}{A_L} \Big) \ . \tag{18}$$

A similar expression can be written for the heavy fragment assuming that the per nucleon kinetic energies of the fragment remain the same as each neutron is emitted,

$$\frac{T_f}{A} = \frac{T_{f1}}{A-1} = \frac{T_{f2}}{A-2} = \cdots \ . \tag{19}$$

The fission product kinetic energy is then $T_p^{\rm tot} = T_L' + T_H'$ If we assume that the same average number of neutrons are emitted by each fragment,

$$\overline{\nu}_L = \overline{\nu}_H = \frac{\overline{\nu}}{2} \ , \tag{20}$$

the average fission product kinetic energy is

$$\langle T_p^{\rm tot} \rangle = \langle T_f^{\rm tot} \rangle \Big[1 - \frac{\overline{\nu}}{2} \Big(\frac{\langle T_L \rangle}{\langle T_f^{\rm tot} \rangle} \frac{1}{\langle A_L \rangle} + \frac{\langle T_H \rangle}{\langle T_f^{\rm tot} \rangle} \frac{1}{\langle A_H \rangle} \Big) \Big] \ . \tag{21}$$

Conservation of momentum tells us that the average kinetic energies per nucleon of the light and heavy fragments are $\langle T_L \rangle / \langle A_L \rangle = (\langle A_H \rangle / \langle A_L \rangle)(\langle T_f^{\rm tot} \rangle / A)$ and $\langle T_H \rangle / \langle A_H \rangle = (\langle A_L \rangle / \langle A_H \rangle)(\langle T_f^{\rm tot} \rangle / A)$ respectively [2] so that finally

$$\langle T_p^{\rm tot} \rangle = \langle T_f^{\rm tot} \rangle \Big[1 - \frac{\overline{\nu}}{2A} \Big(\frac{\langle A_H \rangle}{\langle A_L \rangle} + \frac{\langle A_L \rangle}{\langle A_H \rangle} \Big) \Big] \ . \tag{22}$$

The energy range over which the fission product kinetic energies are available are rather limited for ^{235}U and ^{239}Pu, $E_n < 9$ MeV and $E_n < 5$ MeV respectively [1]. For these isotopes, a linear fit to the data in this energy range is sufficient. The statistics are also rather limited for ^{235}U. On the

other hand, the data for ^{238}U have both higher statistics and a wider energy reach, $1 < E_n < 30$ MeV. These data are sufficiently accurate to exhibit second $(n, n'f)$ and third $(n, n'n''f)$ chance fission (one and two pre-scission neutron emission) at around 6 and 12 MeV. They also deviate from a linear approximation: a quadratic fit is made to these data. The nonlinear quality of the ^{238}U data becomes apparent for energies beyond the range of the ^{235}U and ^{239}Pu data. Thus it is not clear that the linear approximation will hold for these isotopes beyond the range of the fit. Madland's fits to the three isotopes,

$$^{235}\mathrm{U} : \langle T_p^{\mathrm{tot}} \rangle = 169.13 - 0.2660 E_n \ , \tag{23}$$

$$^{238}\mathrm{U} : \langle T_p^{\mathrm{tot}} \rangle = 169.8 - 0.3230 E_n + 0.004206 E_n^2 \ , \tag{24}$$

$$^{239}\mathrm{Pu} : \langle T_p^{\mathrm{tot}} \rangle = 175.55 - 0.4566 E_n \ , \tag{25}$$

are shown up to $E_n = 20$ MeV in Fig. 1. Note the difference in curvature between the linear ^{235}U and the quadratic ^{238}U fits. The extrapolated slope of ^{239}Pu is considerably steeper than that of the U isotopes.

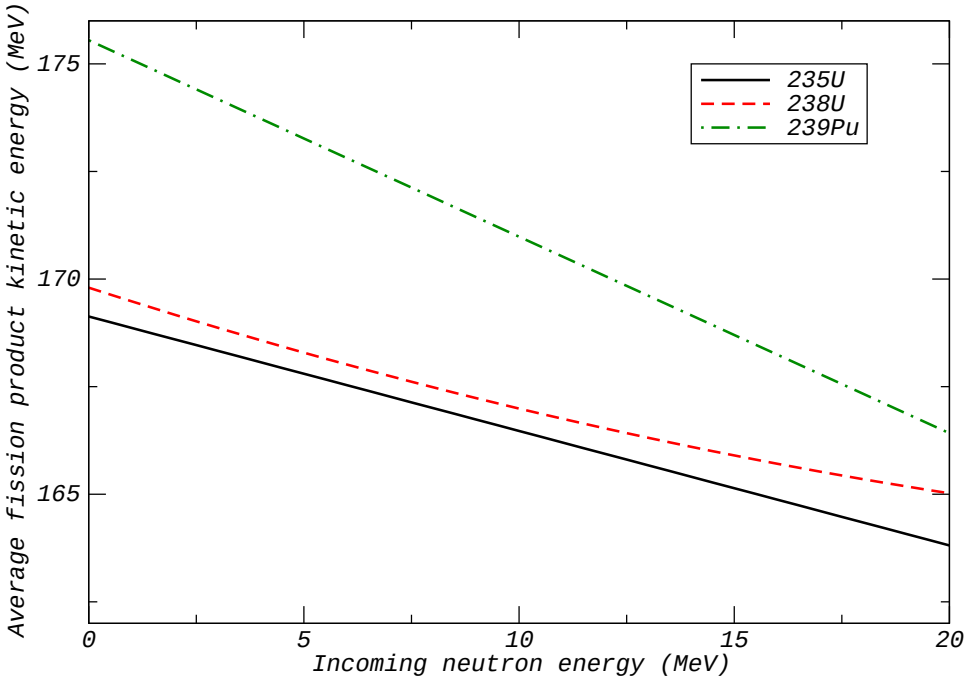

Figure 1: The kinetic energy of the final fission products is given for ^{235}U (solid), ^{238}U (dashed) and ^{239}Pu (dot-dashed).

Since $\overline{\nu}/A$ is small, Eq. (22) can be inverted to obtain the average kinetic energies of the primordial fission fragments,

$$\langle T_f^{\mathrm{tot}} \rangle = \langle T_p^{\mathrm{tot}} \rangle \left[1 + \frac{\overline{\nu}}{2A} \left(\frac{\langle A_H \rangle}{\langle A_L \rangle} + \frac{\langle A_L \rangle}{\langle A_H \rangle} \right) \right] \ . \tag{26}$$

The fragment kinetic energies are 2-3 MeV higher than the product kinetic energies, not surprising since the neutron energies are effectively added back in. Note also that the slopes are weaker and the quadratic coefficient in ^{238}U is reduced,

$$^{235}\mathrm{U} : \langle T_f^{\mathrm{tot}} \rangle = 170.93 - 0.1544 E_n \ , \tag{27}$$

$$^{238}\mathrm{U} : \langle T_f^{\mathrm{tot}} \rangle = 171.70 - 0.2396 E_n + 0.003434 E_n^2 \ , \tag{28}$$

$$^{239}\mathrm{Pu} : \langle T_f^{\mathrm{tot}} \rangle = 177.80 - 0.3489 E_n \ . \tag{29}$$

The dependence of the fission fragment kinetic energy on E_n is shown in Fig. 2.

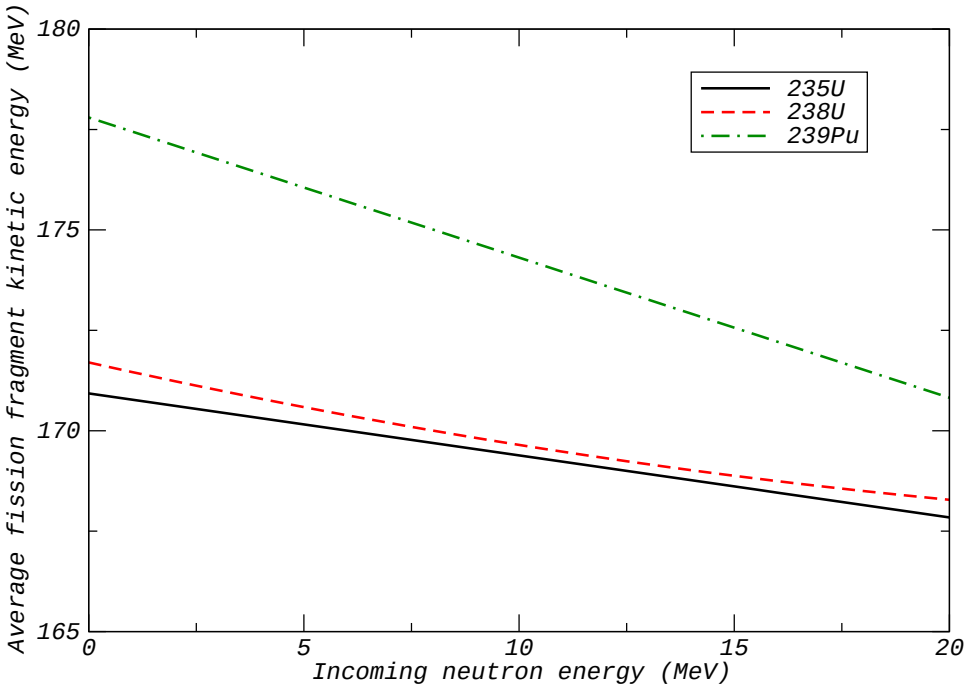

Figure 2: The kinetic energy of the initial fission fragments is given for ^{235}U (solid), ^{238}U (dashed) and ^{239}Pu (dot-dashed).

Note that both the average fission fragment and fission product kinetic energies decrease with E_n. This is because binary fission becomes more symmetric ($\langle A_L \rangle$ and $\langle A_H \rangle$ become closer to $A/2$) as the incident energy increases, thus minimizing the summed fragment and product kinetic energies.

We now discuss how the excitation energy of the fragments is dissipated. This occurs through prompt neutron and gamma emission, as stated earlier,

$$\langle E_{\mathrm{tot}}^* \rangle = \langle E x_n^{\mathrm{tot}} \rangle + \langle E_\gamma^{\mathrm{tot}} \rangle \ . \tag{30}$$

The average fission fragment excitation energy resulting in prompt neutron emission is given by [2]

$$\langle E x_n^{\mathrm{tot}} \rangle = \overline{\nu} [\langle S_n \rangle + \langle \epsilon \rangle] \tag{31}$$

where $\langle S_n \rangle$ is the average neutron separation energy and ϵ is the average center of mass energy of the emitted neutrons.

Several steps go into the evaluation of Eq. (31). The energy dependence of the average prompt neutron multiplicity is taken from the ENDF database. The multiplicities increase almost linearly with neutron energy, as may be expected since more excited fragments can emit more neutrons. The dependence is very similar for ^{235}U and ^{238}U. The ^{239}Pu multiplicity is about 15% higher than the uranium isotopes.

The average fragment neutron separation energy depends on the Z and A of the fragments. An average light and heavy fragment combination is selected for each fissioning compound nucleus, *e.g.* for ^{235}U, $\langle A_L \rangle = ^{96}$Sr and $\langle A_H \rangle = ^{140}$Xe [2]. To reduce the effects of the pairing term in the fragment binding energy, the separation energy for each fragment is obtained by calculating the two neutron separation energy for the fragment central value and six near-neighbor nuclei. The sum of the two-neutron separation energies from both fragments is then divided by four [1]. The result [2] is

$$^{235}\mathrm{U} : \langle S_n \rangle = 4.998\,\mathrm{MeV}\ , \tag{32}$$

$$^{238}\mathrm{U} : \langle S_n \rangle = 4.915\,\mathrm{MeV}\ , \tag{33}$$

$$^{239}\mathrm{Pu} : \langle S_n \rangle = 5.375\,\mathrm{MeV}\ . \tag{34}$$

While a constant value is assumed here, it is worth noting that, since fission tends to be more symmetric as the neutron energy increases, $\langle S_n \rangle$ could be a weak function of incident neutron energy.

Finally, we address the average center-of-mass energy of the prompt neutrons, $\langle \epsilon \rangle$. The calculation of $\langle \epsilon \rangle$ takes multiple chance fission into account. Non-zero probability is assumed for first, second and third chance fission so that $P_f^A = P_{f1}^A + P_{f2}^A + P_{f3}^A$. We note that just because the energy may be high enough for multiple chance fission does not exclude the possibility of first chance fission [2]. In general, the neutron energy moments in the center-of-mass frame of the compound nucleus are,

$$\langle \epsilon_i^n \rangle = \frac{\int_0^\infty d\epsilon \epsilon^n \Phi(\epsilon)}{\int_0^\infty d\epsilon \Phi(\epsilon)}\ , \tag{35}$$

where Φ is normalized so that the integral in the denominator of Eq. (35) is equal to unity ($\langle \epsilon^n \rangle \equiv 1$ for $n = 0$). For first chance fission, only the prompt neutrons after fission need to be accounted for and, if no pre-scission emission occurs, $\langle \epsilon \rangle = \langle \epsilon_1 \rangle$ where $\langle \epsilon_1 \rangle$ is the average center-of-mass neutron energy for first-chance fission. In multiple-chance fission, the kinetic energies of the i neutrons emitted pre-scission have to be included in the neutron kinetic energy, along with the energies of the $\overline{\nu}$ neutrons emitted by the excited fission fragments. Including multiple-chance fission then, the average center-of-mass energy of the prompt fission neutrons is [1]

$$\langle \epsilon \rangle = \frac{P_{f1}^A \overline{\nu}_{f1} \langle \epsilon_1 \rangle + P_{f2}^A [\langle \xi_1 \rangle + \overline{\nu}_{f2} \langle \epsilon_2 \rangle] + P_{f3}^A [\langle \xi_1 \rangle + \langle \xi_2 \rangle + \overline{\nu}_{f3} \langle \epsilon_3 \rangle]}{P_{f1}^A \overline{\nu}_{f1} + P_{f2}^A [1 + \overline{\nu}_{f2}] + P_{f3}^A [2 + \overline{\nu}_{f3}]}\ . \tag{36}$$

Here $\overline{\nu}_{fi}$ is the prompt neutron multiplicity from the $i^{\rm th}$ chance fission, $\langle\epsilon_i\rangle$ is the average neutron center-of-mass energy for $i^{\rm th}$ chance fission and $\langle\xi_{i-1}\rangle$ are the kinetic energies of the pre-scission neutrons emitted in $i^{\rm th}$ chance fission. The calculated values of $\langle\epsilon\rangle$ shown in Fig. 9 of Ref. [1] is a slowly increasing function of E_n, about 20% for $E_n \leq 15$ MeV. Its increase is nonlinear due to the onset of second and third chance fission which slows the growth at the multiple-chance fission thresholds.

Putting these contributions to the prompt neutron center-of-mass emission energy together gives

$$^{235}\mathrm{U} : \langle Ex_n^{\rm tot}\rangle = 14.59 + 0.9772E_n \ , \quad (37)$$

$$^{238}\mathrm{U} : \langle Ex_n^{\rm tot}\rangle = 14.11 + 0.9839E_n \ , \quad (38)$$

$$^{239}\mathrm{Pu} : \langle Ex_n^{\rm tot}\rangle = 19.23 + 1.0707E_n \ , \quad (39)$$

shown in Fig. 3. Note that, despite the nonlinear behavior of $\langle\epsilon\rangle$ with energy, since $\langle S_n\rangle > \langle\epsilon\rangle$ and $\overline{\nu}$ is nearly linear in E_n, $\langle Ex_n^{\rm tot}\rangle$ can be well approximated by a linear fit.

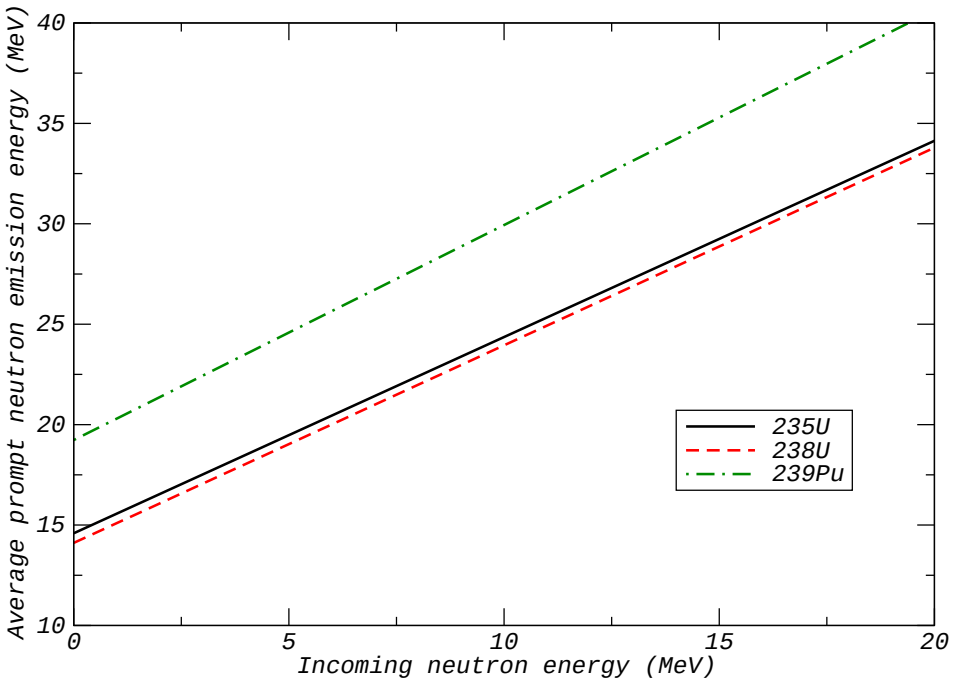

Figure 3: The prompt neutron emission energy in the center-of-mass frame is given for ^{235}U (solid), ^{238}U (dashed) and ^{239}Pu (dot-dashed).

While $\langle Ex_n^{\rm tot}\rangle$ is rather model dependent, there is data for the prompt fission gamma energy, $\langle E_\gamma^{\rm tot}\rangle$ from ^{235}U and ^{239}Pu. An empirical linear fit based n+^{237}Np measurements is used for ^{238}U. While the ^{235}U data are fairly consistent with a linear increase in average prompt gamma energy, the ^{239}Pu

data require a small quadratic term to reduce the increase of $\langle E_\gamma^{\rm tot}\rangle$ with energy. The parameterizations of the average prompt gamma energy are

$$^{235}\mathrm{U} : \langle E_\gamma^{\rm tot}\rangle = 6.600 + 0.0777 E_n \ , \tag{40}$$
$$^{238}\mathrm{U} : \langle E_\gamma^{\rm tot}\rangle = 6.680 + 0.1239 E_n \ , \tag{41}$$
$$^{239}\mathrm{Pu} : \langle E_\gamma^{\rm tot}\rangle = 6.741 + 0.1165 E_n - 0.0017 E_n^2 \ , \tag{42}$$

shown in Fig. 4. We note that this energy is for all prompt gamma emission. The number of emitted gammas is unknown.

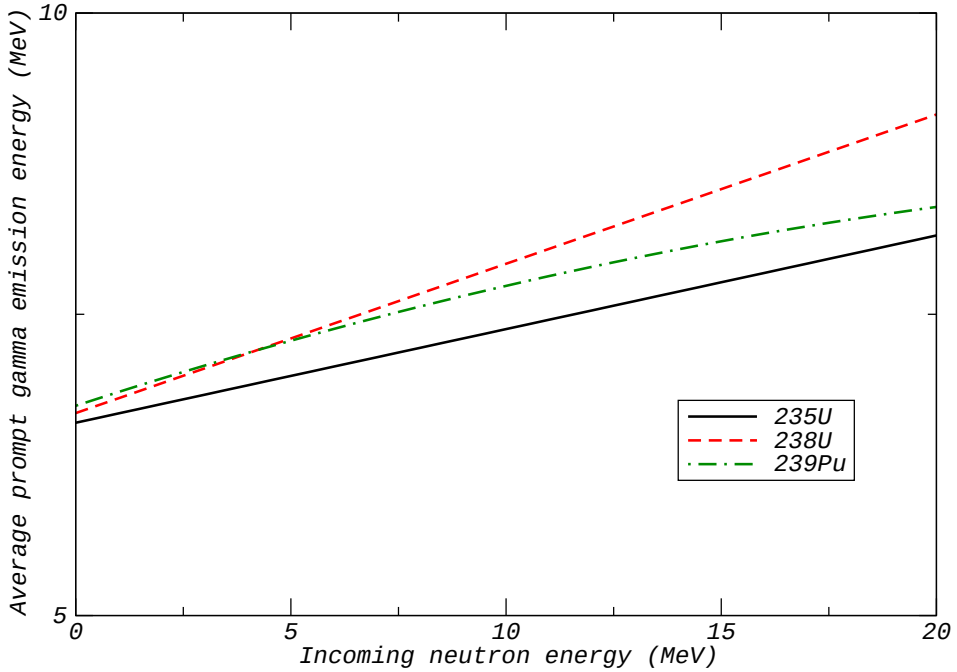

Figure 4: The prompt gamma emission energy is given for ^{235}U (solid), ^{238}U (dashed) and ^{239}Pu (dot-dashed).

The average prompt fission energy release is obtained by substituting Eq. (30) into Eq. (14). Then

$$\langle E_r\rangle = \langle T_f^{\rm tot}\rangle + \langle E x_n^{\rm tot}\rangle + \langle E_\gamma^{\rm tot}\rangle - E_n - B_n \ . \tag{43}$$

Inserting Eqs. (27)-(29), (37)-(39) and (40)-(42) into Eq. (43) with the neutron binding energies

$$^{235}\mathrm{U} : B_n = 6.545\,\mathrm{MeV} \tag{44}$$
$$^{238}\mathrm{U} : B_n = 4.806\,\mathrm{MeV} \tag{45}$$
$$^{239}\mathrm{Pu} : B_n = 6.534\,\mathrm{MeV} \ , \tag{46}$$

for each of the three isotopes, we have

$$^{235}\mathrm{U} : \langle E_r \rangle = 185.6 - 0.0995 E_n \ , \tag{47}$$

$$^{238}\mathrm{U} : \langle E_r \rangle = 187.7 - 0.1318 E_n + 0.0034 E_n^2 \ , \tag{48}$$

$$^{239}\mathrm{Pu} : \langle E_r \rangle = 197.2 - 0.1617 E_n - 0.0017 E_n^2 \ . \tag{49}$$

The average energy release is shown in Fig. 5 for the three isotopes. It is a very slow function of E_n and is, indeed, nearly constant for ^{238}U. The release is largest for ^{239}Pu which also has the greatest dependence on E_n.

The slight decrease in energy release with increasing neutron energy may seem counterintuitive but is a natural consequence of the decrease of the average fission fragment kinetic energies. While both the components of the excitation energy increase with E_n, these contributions are both much smaller than the kinetic energy and do not increase enough to offset the overall downward trend.

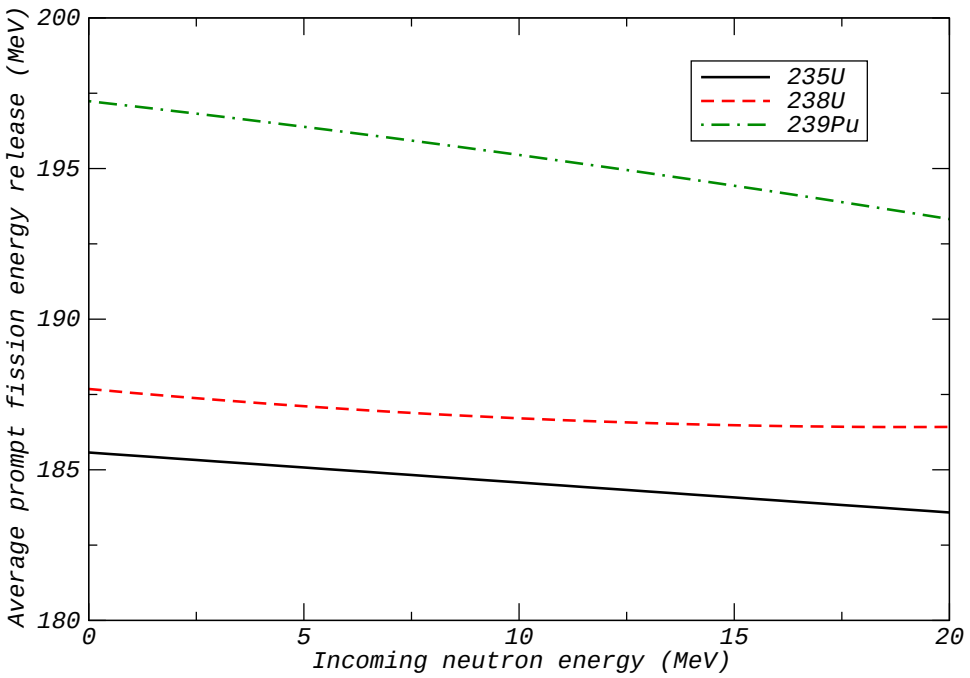

Figure 5: The prompt fission energy release is given for ^{235}U (solid), ^{238}U (dashed) and ^{239}Pu (dot-dashed).

From the energy release, we can determine the energy deposited into the medium, one step closer to obtaining the average fission Q value as a function of energy. The binding energy of the prompt neutrons, $\overline{\nu}\langle S_n \rangle$, is not deposited in the medium and is thus not included in the deposited energy. The average energy deposited in the medium includes the average energy release, $\langle E_r \rangle$,

and the energy introduced into the system by the fission-inducing particle, $E_n + B_n$ for neutron-induced fission,

$$\begin{aligned} \langle E_d \rangle &= \langle E_r \rangle + E_n + B_n - \overline{\nu}\langle S_n \rangle & (50) \\ &= \langle T_f^{\rm tot} \rangle + \overline{\nu}\langle \epsilon \rangle + \langle E_\gamma^{\rm tot} \rangle \ . & (51) \end{aligned}$$

It is preferable to define $\langle E_d \rangle$ solely in terms of measured quantities. This can be done if we replace the average fission fragment kinetic energy by the average fission product kinetic energy using Eq. (26). The energy deposition is then

$$\langle E_d \rangle = \langle T_p^{\rm tot} \rangle + \langle E_{\rm neut}^{\rm tot} \rangle + \langle E_\gamma^{\rm tot} \rangle \quad (52)$$

where $\langle E_{\rm neut}^{\rm tot} \rangle$ is the total prompt fission neutron kinetic energy in the laboratory frame. This energy also includes prompt neutron kinetic energy due to the motion of the fission fragments which emit the neutrons, not included in the fission fragment excitation energy, $\langle Ex_n^{\rm tot} \rangle$. The prompt neutron laboratory kinetic energy is defined as

$$\begin{aligned} \langle E_{\rm neut}^{\rm tot} \rangle &= \overline{\nu}\Big[\frac{1}{2}\Big(\frac{\langle A_H \rangle}{\langle A_L \rangle}\frac{\langle T_p^{\rm tot} \rangle}{A} + \frac{\langle A_L \rangle}{\langle A_H \rangle}\frac{\langle T_p^{\rm tot} \rangle}{A}\Big) + \langle \epsilon \rangle\Big] & (53) \\ &\approx \overline{\nu}\Big[\frac{1}{2}\Big(\frac{\langle A_H \rangle}{\langle A_L \rangle}\frac{\langle T_f^{\rm tot} \rangle}{A} + \frac{\langle A_L \rangle}{\langle A_H \rangle}\frac{\langle T_f^{\rm tot} \rangle}{A}\Big) + \langle \epsilon \rangle\Big] & (54) \\ &= \overline{\nu}\Big[\frac{1}{2}\Big(\frac{\langle T_L \rangle}{\langle A_L \rangle} + \frac{\langle T_H \rangle}{\langle A_H \rangle}\Big) + \langle \epsilon \rangle\Big] & (55) \\ &= \overline{\nu}\langle E \rangle \ . & (56) \end{aligned}$$

The average fission product kinetic energies appear in Eq. (53) because of the way $\langle T_f^{\rm tot} \rangle$ is defined in Eq. (26). In going from Eq. (53) to Eq. (54), Madland assumes that $\langle T_p^{\rm tot} \rangle / A \approx \langle T_f^{\rm tot} \rangle / A$ since $\langle A_L \rangle$ and $\langle A_H \rangle$ are not unique and $\langle \epsilon \rangle > \langle T_L \rangle / \langle A_L \rangle$, $\langle T_H \rangle / \langle A_H \rangle$. The average laboratory neutron energy for multiple chance fission, $\langle E \rangle$ in Eq. (56), is given by

$$\langle E \rangle = \frac{P_{f1}^A \overline{\nu}_{f1}\langle E_1 \rangle + P_{f2}^A[\langle \xi_1 \rangle + \overline{\nu}_{f2}\langle E_2 \rangle] + P_{f3}^A[\langle \xi_1 \rangle + \langle \xi_2 \rangle + \overline{\nu}_{f3}\langle E_3 \rangle]}{P_{f1}^A \overline{\nu}_{f1} + P_{f2}^A[1 + \overline{\nu}_{f2}] + P_{f3}^A[2 + \overline{\nu}_{f3}]} \quad (57)$$

where the average center-of-mass energies for the $i^{\rm th}$ chance fission, $\langle \epsilon_i \rangle$ are replaced by the average laboratory energies $\langle E_i \rangle$. The dependence of $\langle E \rangle$ on E_n is shown in Ref. [1]. The value of $\langle E \rangle$ at $E_n = 0$ and 15 MeV almost identical due to the dips in $\langle E \rangle$ at the second and third chance fission thresholds. The value of $\langle E \rangle$ increases a few percent before the second and third chance fission thresholds and then, at the thresholds, decreases again to near its value at $E_n = 0$. Thus, when this approximately constant function is multiplied by the near-linear dependence of $\overline{\nu}$, the resulting $\langle E_{\rm neut}^{\rm tot} \rangle$ can be approximated by a linear fit,

$$\begin{aligned} {}^{235}{\rm U} : \langle E_{\rm neut}^{\rm tot} \rangle &= 4.838 + 0.3004 E_n \ , & (58) \\ {}^{238}{\rm U} : \langle E_{\rm neut}^{\rm tot} \rangle &= 4.558 + 0.3070 E_n \ , & (59) \\ {}^{239}{\rm Pu} : \langle E_{\rm neut}^{\rm tot} \rangle &= 6.128 + 0.3428 E_n \ . & (60) \end{aligned}$$

The energy dependence of $\langle E^{\rm tot}_{\rm neut}\rangle$ is shown in Fig. 6.

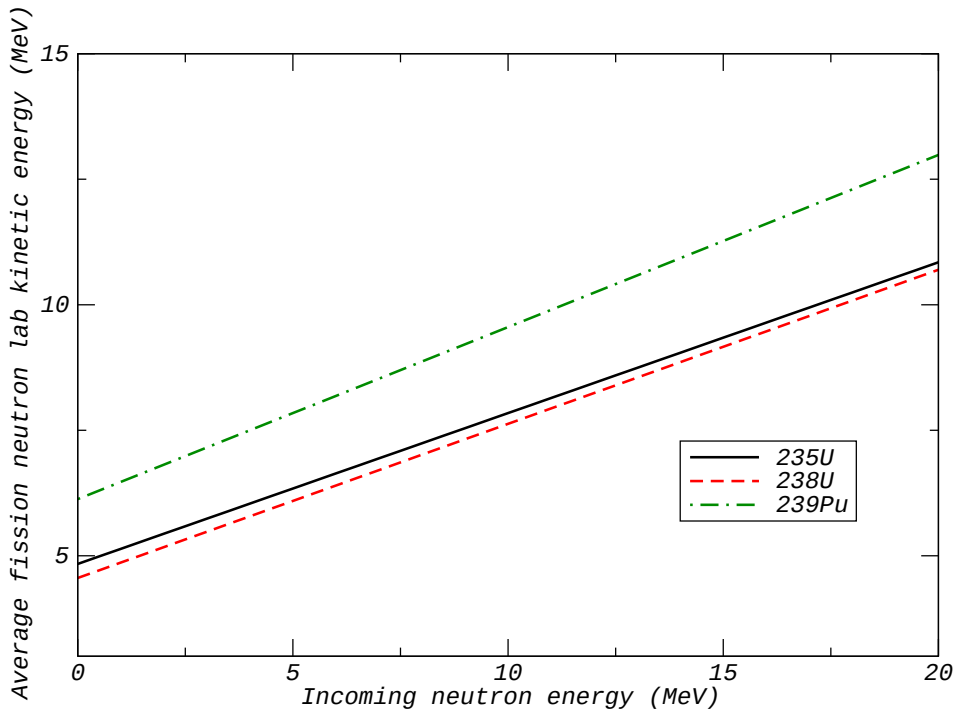

Figure 6: The prompt fission neutron kinetic energy in the laboratory frame is given for ^{235}U (solid), ^{238}U (dashed) and ^{239}Pu (dot-dashed).

Combining Eqs. (23)-(25), (40)-(42) and (58)-(60) in Eq. (52) gives the average fission energy deposition,

$$^{235}\mathrm{U} : \langle E_d\rangle = 180.57 + 0.1121E_n \ , \tag{61}$$

$$^{238}\mathrm{U} : \langle E_d\rangle = 181.04 + 0.1079E_n + 0.0042E_n^2 \ , \tag{62}$$

$$^{239}\mathrm{Pu} : \langle E_d\rangle = 188.42 + 0.0027E_n - 0.0017E_n^2 \ , \tag{63}$$

shown in Fig. 7. The average energy deposition is smaller than the energy release and has a different dependence on E_n, particularly for the uranium isotopes. The value for ^{239}Pu is larger and nearly independent of E_n. On the other hand, $\langle E_d\rangle$ increases slowly with energy for both ^{235}U and ^{238}U with a larger increase seen for ^{238}U. The difference in the E_n dependence of $\langle E_d\rangle$ and $\langle E_r\rangle$ can best be seen by examination of Eq. (50). The decrease of $-\overline{\nu}\langle S_n\rangle$ with E_n is slower than E_n increases, causing the increase of $\langle E_d\rangle$ with E_n for the uranium isotopes. Since $\langle E_r\rangle$ for ^{239}Pu is almost 10 MeV larger, the difference $E_n - \overline{\nu}\langle S_n\rangle$ has a smaller effect, reducing the decrease but not resulting in a corresponding increase.

Finally, the fission Q value is the difference between the energy deposited and the incident neutron energy,

$$Q(E_n) = \langle E_d\rangle - E_n \ . \tag{64}$$

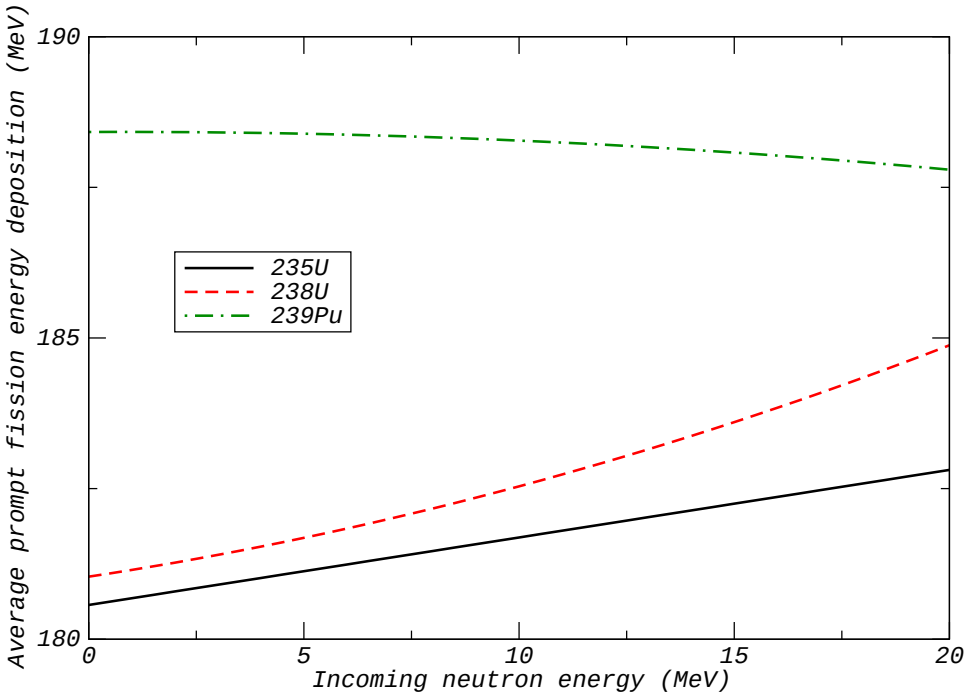

Figure 7: The energy deposition is given for ^{235}U (solid), ^{238}U (dashed) and ^{239}Pu (dot-dashed).

The parameterizations for the three isotopes, obtained by subtracting E_n from Eqs. (61)-(63),

$$^{235}\mathrm{U} : Q(E_n) = 180.57 - 0.8879E_n \ , \tag{65}$$

$$^{238}\mathrm{U} : Q(E_n) = 181.04 - 0.8921E_n + 0.0042E_n^2 \ , \tag{66}$$

$$^{239}\mathrm{Pu} : Q(E_n) = 188.42 - 0.9973E_n - 0.0017E_n^2 \ , \tag{67}$$

are shown in Fig. 8. All three isotopes exhibit a decrease in Q with E_n, as may be expected for more symmetric fission with increasing E_n.

2 Implementation

Introducing an energy dependent Q value may well lead to inconsistencies with the fission neutron and gamma energies (`I=10`) for `iyo=1` and 7 in the ENDL99 database since the fission Q value has been assumed to be constant. This can be checked by comparing the current ENDL99 values with Madland's results [1], described here, and with the latest ENDF release, ENDF/B-VII.0 [3], which has, to some extent, incorporated Madland's parameterizations.

The new ENDF release did not fully incorporate the dependence of the energy release, $\langle E_r \rangle$, and prompt gamma emission energy, $\langle E_\gamma^{\mathrm{tot}} \rangle$, on incident

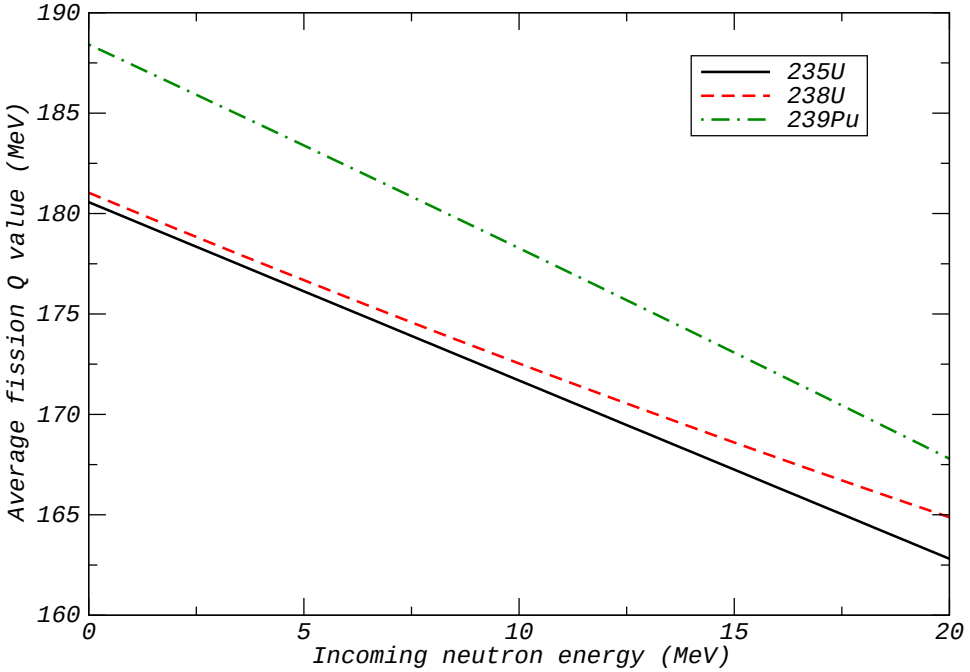

Figure 8: The energy dependence of the fission Q value is given for ^{235}U (solid), ^{238}U (dashed) and ^{239}Pu (dot-dashed).

neutron energy as parameterized by Madland since that would have entailed modifying the database structure. Since this would have delayed the release, these values were left independent of E_n [3].

The energy dependence of the quantities shown in section 1 can be summarized as

$$E_i(E_n) = c_0 + c_1 E_n + c_2 E_n^2 \ . \tag{68}$$

The value of c_0 for $E_i = E_r$ and $E_i = E_\gamma^{\rm tot}$ obtained by Madland for the three isotopes discussed here were implemented in ENDF/B-VII.0 for the entire energy range. Thus the Madland and ENDF/B-VII.0 values for the energy release and the total prompt gamma emission energy only agree at $E_n = 0$.

On the other hand, the prompt neutron emission energy is rather well measured and is proportional to the average prompt neutron multiplicity, see Eq. (56). The values obtained from fits to the data at $E_n = 0.0253$ eV are 1.6% higher, 5.4% higher and $\sim$ 1% lower than Madland's results for ^{235}U, ^{238}U and ^{239}Pu respectively. To maintain consistency with these data, in ENDF/B-VII.0 the data for $E_{\rm neut}^{\rm tot}(E_n)$ are used instead of Madland's parameterization.

Figures 9-11 compare Madland's parameterizations of the energy dependence of $\overline{\nu}$, $\langle E_{\rm neut}^{\rm tot}\rangle$ and $\langle E_\gamma^{\rm tot}\rangle$ with the ENDF/B-VII.0 and the ENDL99 databases.

We first show the prompt neutron multiplicity as a function of incident neutron energy in Fig. 9. The energy dependence of $\overline{\nu}$ can be obtained from Eq. (50),

$$\overline{\nu} = \frac{1}{\langle S_n \rangle}(\langle E_r \rangle + E_n + B_n - \langle E_d \rangle) \ , \tag{69}$$

assuming that $\langle S_n \rangle$ is constant. The comparison is shown in Fig. 9. Both the ENDF/B-VII.0 and ENDL99 (`I=7` for `iyo=1`) values are in rather good agreement with Eq. (69) for $E_n < 15$ MeV.

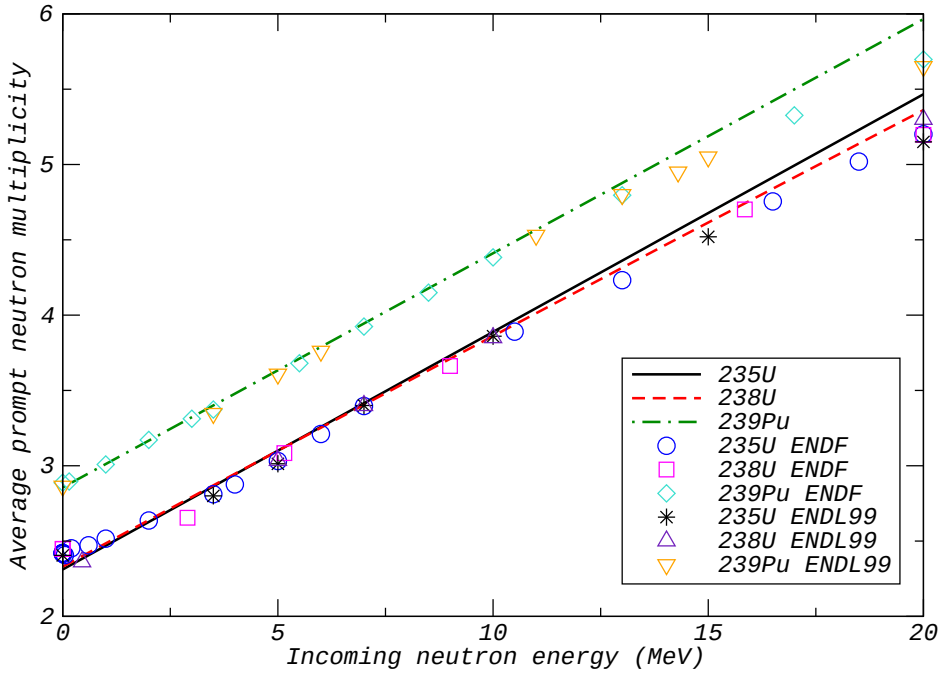

Figure 9: The model prompt fission neutron multiplicity for ^{235}U (solid), ^{238}U (dashed) and ^{239}Pu (dot-dashed) is compared with the ENDF/B-VII.0 (^{235}U, blue circles; ^{238}U, magenta squares; and ^{239}Pu, green diamonds) and ENDL99 (^{235}U, black stars; ^{238}U, purple upward-pointing triangles; and ^{239}Pu, orange downward-pointing triangles) databases.

Figure 10 compares Eq. (53) with ENDF/B-VII.0 and ENDL99 (`I=10` for `iyo=1`) for all three isotopes. The ENDF/B-VII.0 data agree rather well with Eq. (53) for $E_n < 15$ MeV. This is not surprising since the ENDF/B-VII.0 result is obtained from Eq. (56) with $\overline{\nu}$ as in Fig. 9. On the other hand, the ENDL99 energy dependence is much stronger for ^{235}U and ^{239}Pu. While the low E_n ENDL99 points lie somewhat below the curves, above $E_n = 10$ MeV the ENDL99 points are substantially above the curves. It is unclear whether the ENDL99 ^{235}U data would follow this trend at higher energy

since the highest point is at $E_n \sim 7$ MeV. Given the small discrepancies between the ENDF/B-VII.0 and Madland implementations of $E^{\rm tot}_{\rm neut}(E_n)$, it seems sufficient to use the ENDF/B-VII.0 result.

On the other hand, the prompt gamma energy from ENDL99, ENDF/B-VII.0 and Madland, shown in Fig. 11, are quite different. The constant energy assumed in ENDF/B-VII.0 is quite different from the ENDL99 points, (`I=10` for `iyo = 7`), which have a much stronger energy dependence than given in Eqs. (40)-(42). Future releases of the ENDF database will likely more completely incorporate the Madland results for $\langle E^{\rm tot}_\gamma \rangle$.

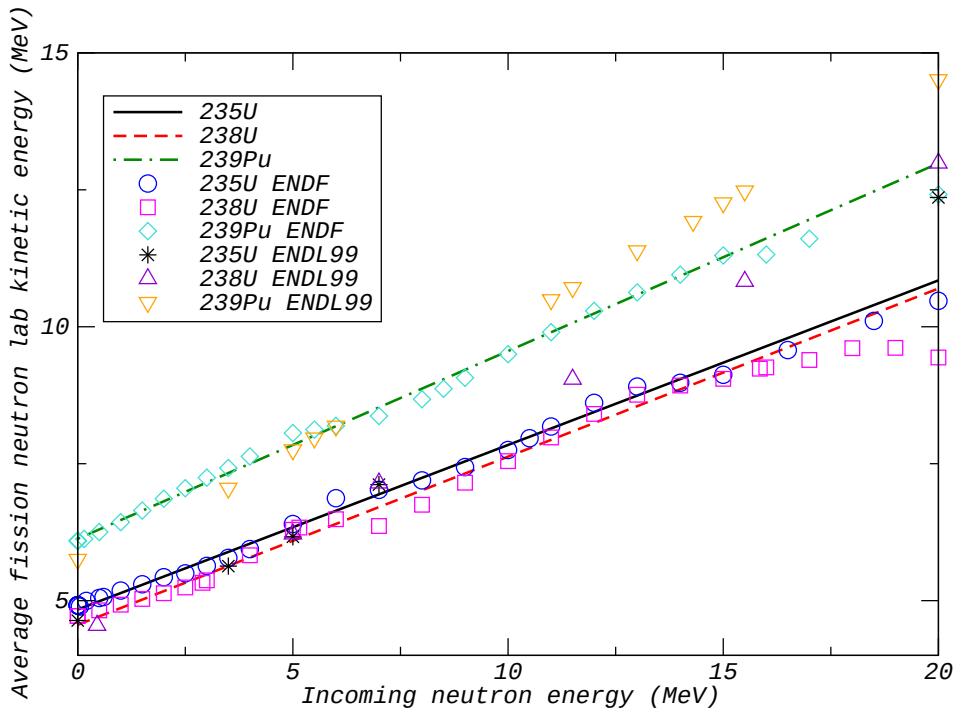

Figure 10: The model average prompt neutron energy in the lab frame for ^{235}U (solid), ^{238}U (dashed) and ^{239}Pu (dot-dashed) is compared with the ENDF/B-VII.0 (^{235}U, blue circles; ^{238}U, magenta squares; and ^{239}Pu, green diamonds) and ENDL99 (^{235}U, black stars; ^{238}U, purple upward-pointing triangles; and ^{239}Pu, orange downward-pointing triangles) databases.

The total prompt energy deposited in fission as a function of incident neutron energy, $E_d(E_n)$, in ENDF/B-VII.0 is finally very similar to Madland's parameterization over the entire incident neutron energy range even though ENDF/B-VII.0 only includes the energy dependence of the prompt neutron spectrum. This occurs because the higher constant ENDF/B-VII.0 value of the average energy release compensates for the lower values of $E^{\rm lab}_{\rm neut}(E_n)$ and $\langle E^{\rm tot}_\gamma \rangle$ in ENDF/B-VII.0 relative to the Madland parameterization. At $E_n = 14$ MeV, the ENDF/B-VII.0 values of E_d, related to the fission Q value, are all within 1% of Madland's results.

To maintain consistency with the energy dependent Q values obtained here, the translated ENDF/B-VII.0 values for `I=10` should be used instead of the current ENDL99 values. Otherwise energy conservation is not exact. The next ENDL release will incorporate these `I=10` files?

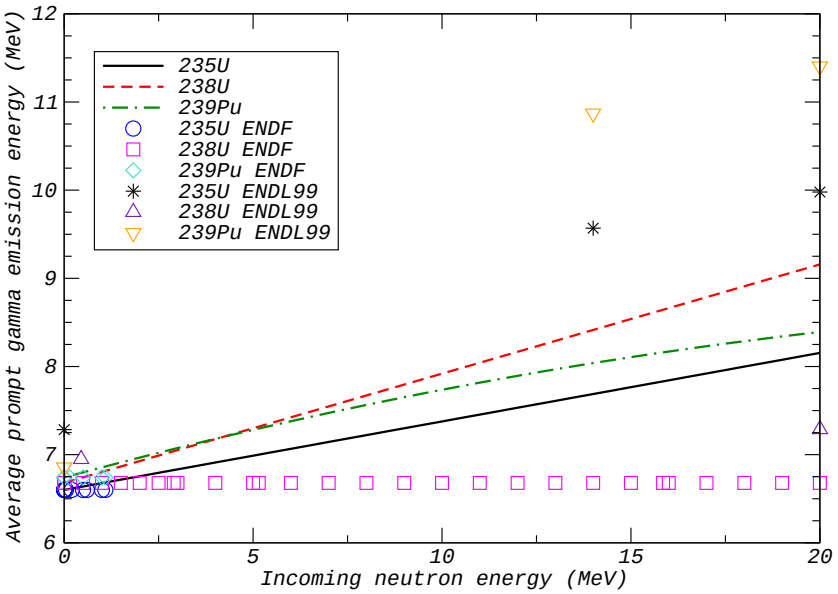

Figure 11: The model average prompt gamma energy in the lab frame for ^{235}U (solid), ^{238}U (dashed) and ^{239}Pu (dot-dashed) is compared with the ENDF/B-VII.0 (^{235}U, blue circles; ^{238}U, magenta squares; and ^{239}Pu, green diamonds) and ENDL99 (^{235}U, black stars; ^{238}U, purple upward-pointing triangles; and ^{239}Pu, orange downward-pointing triangles) databases.

In order for user codes such as `MCAPM` to employ the energy-dependent Q values in Eqs. (65)-(67), the ascii data files generated in the calculation must be read, processed and transformed into pdf (Portable Data Binary) format. The code responsible for this is `MCFGEN`. We now describe how this is done.

An additional `I` number, `I=12`, is incorporated for fission. The file `datablk.f` has had `I=12` added to the `irlst` data statement. Then `main.f` was modified to loop over the additional `I` number in the case of the three fissile isotopes parameterized here: $ZA = 92235$ (^{235}U); 92238 (^{238}U); and 94239 (^{239}Pu).

`MCFGEN` then reads the energy-dependent Q values in pointwise ascii format and averages them over the incident-energy groups for each isotope with the chosen flux weighting profile. (In this case, a flat or constant flux was employed for an isotropic profile.) This is done in the routines `sig0av.f` and `iequ0.f` by implementing the call for energy-dependent Q's from `C=5` alone to `C=15` and `C=5`. The group-averaged Q values are then packed into

the structured binary pdb file.

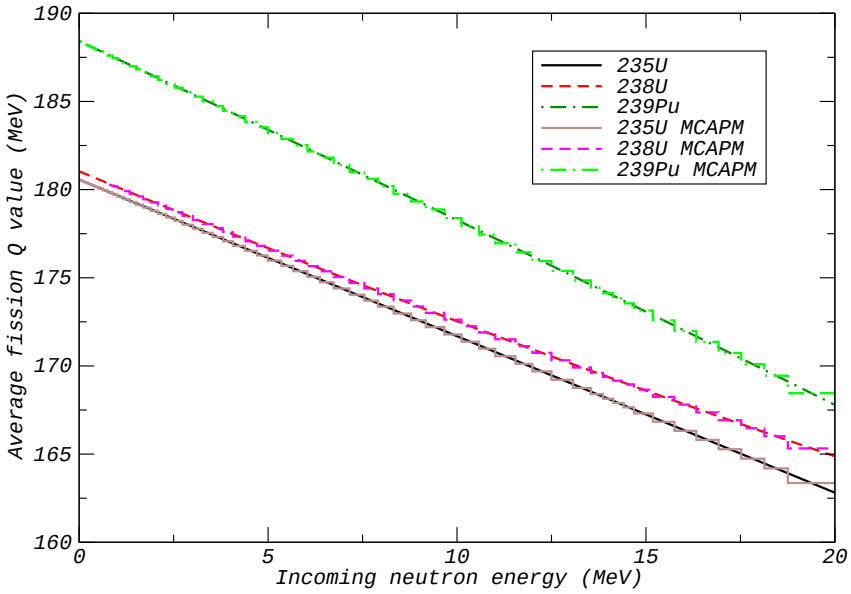

Figure 12: The energy dependence of the fission Q value is given for ^{235}U (solid), ^{238}U (dashed) and ^{239}Pu (dot-dashed). The lines employ Eqs. (65)-(67) while the histograms are the corresponding output from `MCAPM`.

`MCAPM` reads the pdb file and places the Q values in the appropriate array for access via the `Bang2000` collision function or the special access functions. Fig. 12 shows the comparison of the Q values in Eqs. (65)-(67) with the output Q from `MCAPM`. The group averaging of `MCFGEN` is clear, creating a characteristic stepwise pattern in good agreement with Madland's parameterization.

References

[1] D. Madland, Nucl. Phys. A **772** (2006) 113.

[2] D. Madland and J. R. Nix, Nucl. Sci. and Eng. **81** (1982) 213.

[3] M. B. Chadwick *et al.*, Nuclear Data Sheets **107** (2006) 2931.